

Effect of the addition of polyester-grafted-cellulose nanocrystals on the shape memory properties of biodegradable PLA/PCL nanocomposites



Valentina Sessini ^{a, *}, Iván Navarro-Baena ^b, Marina P. Arrieta ^c, Franco Dominici ^b, Daniel López ^c, Luigi Torre ^b, José M. Kenny ^b, Philippe Dubois ^a, Jean-Marie Raquez ^a, Laura Peponi ^{c, **}

^a Laboratory of Polymeric and Composite Materials, University of Mons – UMONS, Place du Parc 23, 7000, Mons, Belgium

^b Dipartimento di Ingegneria Civile e Ambientale, Università di Perugia, Strada di Pentima, 05100, Terni, Italy

^c Instituto de Ciencia y Tecnología de Polímeros, ICTP-CSIC, Calle Juan de la Cierva 3, 28006, Madrid, Spain

ARTICLE INFO

Article history:

Received 30 November 2017

Received in revised form

16 February 2018

Accepted 9 April 2018

Available online 10 April 2018

Keywords:

Shape memory

Thermally-activated

PLA/PCL blend

Nanocomposites

CNC

ABSTRACT

In this work the thermally-activated shape memory response of biodegradable nanocomposites based on PLA/PCL blend reinforced with different type of cellulose nanocrystals has been reported, and compared with those of the neat matrix, at the same transition temperature of 55 °C and at the same different deformations, 50%, 100% and 150%. In particular, cellulose nanocrystals have been synthesized and then functionalized by “grafting from” reaction by ring opening polymerization of both PLLA and PCL using the –OH groups onto the cellulose nanocrystals surface as initiators for the reaction. The morphology, thermal and mechanical analysis have been performed in order to obtain the parameters for the thermo-mechanical shape memory cycles. Moreover, the addition of the CNC-based nanofillers on the compatibility of PLA-PCL blends in 70:30 proportion has been evaluated. All the biodegradable nanocomposite formulations showed excellent shape memory response, similar to those of the neat matrix, with strain recovery ratio and strain fixity ratio higher than 80% and 90%, respectively. This fact indicates that in this case, the shape memory response of the nanocomposites is mainly controlled by the response of the neat blend and they are slightly influenced by the increase of compatibility between the components of the blend. In addition, all nanocomposite films were fully disintegrated under composting conditions confirming their biodegradable nature, obtaining that the presence of CNC-based nanofillers speeds up the disintegration rate of the nanocomposites in comparison with the pure matrix.

© 2018 Published by Elsevier Ltd.

1. Introduction

The use of biodegradable polymers has been increasing in the last years in several industrial applications in order to prevent the accumulation of plastics waste. Among others, PLA is one of the most used biopolymers due to many advantages such as its

renewable nature, biodegradable character, biocompatibility, high transparency, availability in the market, excellent tensile strength and stiffness equivalent to some commercial petroleum-based polymers [1–3]. However, the use of PLA as film is limited because PLA shows high brittleness and thus several efforts has been focused on PLA modification for extending its industrial application as flexible films, such as plasticization [4,5], blending [6–8] or by copolymerization [9,10].

Blending process is a common and relatively simple way that is currently available at industrial level approach to tune up the physical and mechanical properties of biopolymers. Thus, the modification of PLA by blending with other biodegradable polymers has many advantages, offering the opportunity to improve properties in a wide range, while leading to fully compostable materials with minimal carbon-footprint [11]. Poly(ϵ -caprolactone)

* Corresponding author.

** Corresponding author.

E-mail addresses: valentina.sessini@umons.ac.be (V. Sessini), ivan.navarrobaena@gmail.com (I. Navarro-Baena), marrieta@ictp.csic.es (M.P. Arrieta), francodominici1@gmail.com (F. Dominici), daniel@ictp.csic.es (D. López), luigi.torre@unipg.it (L. Torre), jose.kenny@unipg.it (J.M. Kenny), philippe.dubois@umons.ac.be (P. Dubois), jean-marie.raquez@umons.ac.be (J.-M. Raquez), lpeponi@ictp.csic.es (L. Peponi).

is an interesting biodegradable polymer that has been widely blended with PLA [12], mainly because it offers the opportunity to increase PLA flexibility avoiding plasticizers losses during processing as well as migration phenomenon during service [11].

Some previous studies on PLA/PCL blends-based nanocomposites have been reported using different types of micro- and nano-particles, such as carbon nanotubes [13], clays [14], sepiolite [15], montmorillonite [16], micro-talc [17], carbohydrate nanocrystals [18,19] among others [20], to improve the compatibility between PLA and PCL matrices. In particular, in the last years, cellulose nanocrystals (CNC) have been widely used as reinforcement for PLA [21–23] as well as for PCL [24] due to its biodegradability, renewability and high stiffness. However, the homogeneous dispersion of CNC into PLA and PCL matrices is not easy to achieve due to their very different hydrolytic/hydrophobic response. Thus, CNC functionalization is required to improve the dispersion of the nanofillers in the polymeric matrix as well as the final properties of the nanocomposites [25,26]. The strategy of grafting polymer chains at the surface of the CNC through a “grafting from” approach has been showed to be an effective way to obtain nanocomposites based on CNC and PLA and/or PCL matrices with enhanced final properties [25,27]. Moreover, Goffin et al. [18] reported that the compatibilization of PCL/PLA blends can be strongly affected by the addition of polyester-grafted cellulose nanocrystals.

In our previous work [8] we found that among other properties, PLA blended with 30 wt % PCL shows excellent shape memory properties at 55 °C. In fact, the presence of the right proportion between two different phases such as PLA and PCL was necessary to develop shape memory materials. Shape memory behavior is the capability of a material to recover its original shape from a deformed and fixed temporary one thanks to the application of an external stimulus, such as temperature, humidity, pH and so on [28,29]. In fact, a stable “permanent phase” is required in order to memorize the initial shape and a “switching phase” is needed to fix and recover the temporary and initial shape, respectively. In general, in the thermally-activated shape memory materials, the switching phase is related to a switching temperature (T_{sw}) such as the melting temperature and the glass transition temperature [30]. In the case of PLA/PCL blends, the PCL domain can be the switching phase, whereby T_m of PCL is the switching temperature and the semi-crystalline PLA is considered to be the permanent phase. That is, heating at the T_{sw} is possible to program the temporary shape, which is fixed after quenching the sample at the fixing temperature (T_{fix}) well below the T_{sw} . Finally, to activate the recovery of the initial shape, the T_{sw} has to be reached [31].

In this work, the effect of the addition of different modified and non-modified CNC nanofillers, on the shape memory properties of PLA/PCL blends in 70:30 proportion has been studied in terms of morphology, thermal and mechanical properties in order to correlate them with the shape memory performances of the nanocomposites. Finally, the disintegration under composting conditions at a laboratory-scale level was assayed in order to corroborate their biodegradability.

2. Experimental

2.1. Materials

PLA 3051D (D-lactide content of 4%) with density of 1.25 g/cm³ and a molecular weight (M_n) of about 1.42×10^4 g/mol, was supplied by Nature Works®, USA. PCL CAPA8000 and PCL diol, CAPA2403 ($M_n = 4000$ g mol⁻¹) were kindly donated by Perstorp (Sweden). Microcrystalline cellulose (MCC), L-Lactide, stannous octoate, sulfuric acid, toluene, methanol, ethanol, acetone, chloroform and dichloromethane were purchased from Sigma Aldrich

(Spain).

2.2. Synthesis of cellulose nanocrystals

The cellulose nanocrystals (CNC) were obtained from acid hydrolysis of commercial microcrystalline cellulose (MCC) following a previously reported method [21,32]. In brief, an acid hydrolysis was performed with sulfuric acid (64% (wt/wt)) at 45 °C for 30 min in a 250 ml three-neck round-bottom flask. 20 g of MCC and 175 ml of acid were mixed in the flask and homogenized by mechanical stirring. The obtained product was diluted in 4 L of deionized water to stop the hydrolysis reaction, while the excess of acid was removed by centrifugation. After this process, 1 L of CNC solution was obtained and then the solution was dialyzed for 5 days in order to neutralize it. An ion exchange resin (Dowex Marathon MR-3 hydrogen and hydroxide form) was added for 24 h to the solution in order to purify the solution and it was then removed by filtration. Then, to improve the thermal stability of CNC, the pH of the solution was adjusted to 9.0 using a 1.0% NaOH buffer solution [21]. Finally, the CNC solution was sonicated to get a stable suspension of the nanofillers. The fully crystalline nature of the obtained CNC was confirmed by X-ray analysis.

2.3. CNC functionalization with PLLA or PCL chains

Two surface chemical modifications of the CNC were performed by grafting PLLA chains as well as PCL chains onto the CNC surface by ring opening polymerization (ROP) of L-lactic acid (L-LA) or ϵ -caprolactone (ϵ -CL), respectively, by using the surface hydroxyl groups of the CNC as initiator, as schematically shown in Fig. 1. The procedure for CNC functionalization was previously reported by Bitinis et al. [33] for PLLA grafting and by Paquet et al. [34] for PCL grafting. Briefly, the aqueous suspension of CNC was solvent-exchanged with acetone, then with dichloromethane and finally with previously dried toluene with phosphorus pentoxide. For each solvent exchange step, the solution was centrifuged and re-dispersed three times.

The modification reaction took place in a three-neck round-bottom flask equipped with a condenser with a calcium chloride tube. All the reaction system was kept under nitrogen atmosphere. The monomer was dissolved in dry toluene for 10 min at 50 °C. Then, the CNC in toluene solution were added and the reaction was heated until 80 °C. When the reaction temperature was reached, 0.2 g of Sn(Oct)₂ were added and the reaction got proceed for 24 h. In order to remove the un-reacted monomer and the no-grafted polymer, a centrifugation-redispersion protocol was followed, i.e., 4 cycles of methanol, 4 cycles of ethanol and 2 cycles of acetone. Finally, the modified CNC were dissolved in chloroform to store them. The obtained CNC were named, depending on the polymer functionalization, CNC-g-PLLA and CNC-g-PCL.

2.4. Processing of the PLA/PCL nanocomposites

Nanocomposites based on PLA/PCL blend (70:30) and reinforced with 1 wt % of different CNC-based nanofillers were processed by melt-blending based on our previous work [8]. In particular, in this work we chose to use 1 wt % CNC nanofillers, pristine and functionalized with both PLLA and PCL, in order to study how the different functionalization can affect the final properties of the nanocomposites. In fact, in our previous work we obtained that 1 wt % of PLLA functionalized CNC increased the shape memory response of synthesized polyurethanes [35] even if the addition of nanofillers changed the switching temperature of the polymeric matrix in their shape memory characterization. Prior to the melt-blending of the nanocomposites, the materials were dried in a

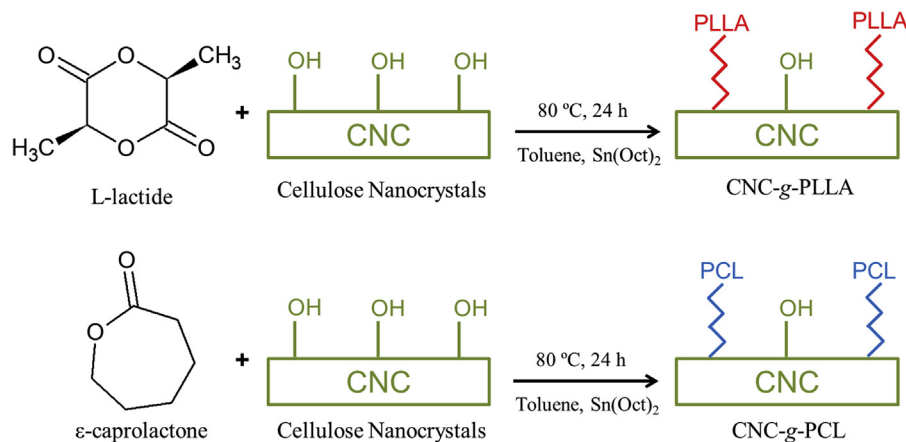


Fig. 1. CNC functionalization with PCL and PLLA polymer chains.

vacuum oven at 40 °C during 24 h. After weighting the materials, the polymeric matrix and the nanofillers were manually pre-mixed and then added to the extruder. All the materials were prepared in a DSM Xplore co-rotating extruder at a screw speed of 100 rpm, at 180 °C at a mixing time of 3 min. After the extrusion process, the materials were further processed by compression molding into films with thickness of about 500 micron in a Dr. Collin 200 mm × 200 mm press at 180 °C. The properties of the nanocomposites were compared to that of the neat blend composed by 70 wt % of PLA and 30% of PCL (M70PLA). The nanocomposites were then named M70PLA/CNC, M70PLA/CNC-g-PLLA and M70PLA/CNC-g-PCL, emphasizing the composition of the blend and the type of CNC used as nanofillers.

2.5. Characterization techniques

The morphology of pristine CNC, CNC-g-PLLA and CNC-g-PCL was studied by Transmission Electron Microscopy (TEM). TEM measurements were performed on the JEOL JEM-2100 TEM instrument (JEOL Ltd., Akishima, Tokyo, Japan), with a LaB6 filament and with an operating voltage of 200 kV. For TEM analysis, the solutions were cast directly on the 200-mesh copper grid followed by solvent evaporation at ambient conditions for 24 h.

Field Emission Scanning Electron Microscope (FE-SEM, Hitachi S8000) in transmission mode was used to study the dispersion of the nanofillers in the polymer matrix while the morphology of the nanocomposites was analyzed by Field Emission Scanning Electron Microscopy (FE-SEM Supra 25, Zeiss). The film samples were immersed in liquid nitrogen and then cryo-fractured. All the samples were gold coated by an Agar automatic sputter coater.

Raman spectra were taken using a Renishaw InVia Reflex Raman system. An optical microscope was coupled to the system. The Raman scattering was excited using a diode laser at a wavelength of 785 nm. The laser beam was focused on the sample with a 100 × 0.85 microscope objective. The laser power at the sample was 350 mW. The exposure was 10 s and 10 accumulations for the Raman measurements.

Fourier transform infrared (FTIR) spectra were obtained in the attenuated total reflectance (ATR) mode. The measurements were performed using a Spectrum One FTIR spectrometer Perkin Elmer equipped with an internal reflection element of diamond in the range of 650–4000 cm⁻¹ with 1 cm⁻¹ of resolution and an accumulation of 16 scans.

Wide-angle X-ray diffraction (WAXD) measurements were performed using a Bruker D8 Advance instrument with a Cu K α source (0.154 nm) and a detector Vantec1. The scanning range was 2°–50°, step-size and count time per step were 0.023851° and 0.5 s, respectively.

The thermal properties were investigated by Differential Scanning Calorimetry (DSC) analysis in a Mettler Toledo DSC822e instrument. Samples of about 10 mg were sealed in aluminum pans. Thermal cycles were composed by three cycles: firstly, a heating scan from 25 °C to 200 °C, to erase the thermal history of the sample and to choose the appropriate temperature to which trigger them (T_{sw}) for shape memory applications. Then, a cooling scan from 200 °C to -90 °C and finally a heating scan from -90 °C to 200 °C. All scans were performed with a heating rate of 10 °C/min, under nitrogen flow (40 ml/min). From these scans were obtained the glass transition temperatures (T_g), the melting temperatures (T_m), the crystallization temperatures (T_c) as well as the crystallization enthalpy (ΔH_c) and the melting enthalpy (ΔH_m). The crystallinity of the samples was calculated according with Equation (1).

$$\chi_c^a = \frac{1}{1 - X^a} \left[\frac{\Delta H_m}{\Delta H_{m0}} \right] \cdot 100 \quad (1)$$

χ_c^a represents the degree of crystallinity of the component a , ΔH_m is the melting enthalpy, ΔH_{m0} is the melting enthalpy for a 100% crystalline material and X^a is the percentage of the crystalline component a in the sample. The value taken for ΔH_{m0} of PCL was 148 KJ/mol, while for PLLA was 93 KJ/mol [36].

Thermogravimetric analysis (TGA) was carried out using a TA-TGA Q500 analyzer. The experiments were performed using about 10 milligrams of sample from room temperature to 600 °C at 10 °C/min under nitrogen atmosphere with a flow of 60 ml/min. The initial degradation temperatures ($T_{5\%}$) were determined at 5% mass loss while the maximum degradation temperatures (T_{max}) were calculated from the first derivative of the TG curves (DTG).

The mechanical properties were determined using an Instron Universal Testing Machine at a strain rate of 200 mm/min according to ISO 37 [37]. Measurements were performed on 5 dog-bone specimens with a width of 2 mm and leaving an initial length between the clamps of 20 mm. From these experiments were obtained the Young Modulus, as the slope of the curve between 0% and 2% of deformation, the elongation at break and the maximum strain reached.

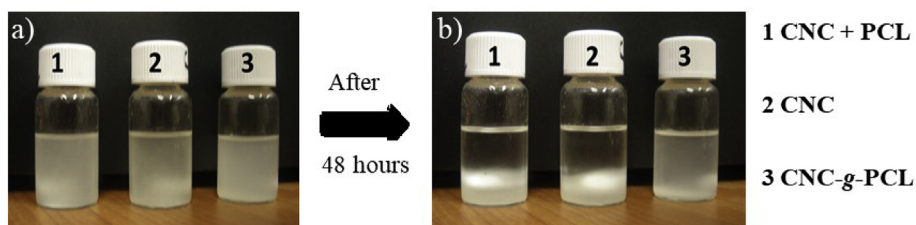


Fig. 2. Suspensions in chloroform 1) mixture of CNC and PCL; 2) pristine CNC; 3) CNC-g-PCL nanofillers just after stopping the stirring (a) and after 48 h of stirring stop (b).

Thermally-activated shape memory characterization was carried out in a Dynamic mechanical thermal analyzer (DMTA) using a DMA Q800 (TA Instrument) in film tension. Thermo-mechanical cycles were performed at a T_{sw} near to the T_m of PCL thus considering that in our system, PLA acts as permanent phase while crystalline PCL is the switching phase. In fact, in order to perform thermally-activated shape memory analysis, it is necessary to heat the sample at the corresponding T_{sw} and to stretch the sample to a desired shape. Then, the material is cooled while maintaining the deformation. Once the applied stress is removed, the recovery of the original shape occurs by re-heating the sample at the T_{sw} . Therefore, in order to analyse the effects of the addition of CNC and functionalized CNC on the thermally-activated shape memory response of the PLA/PCL blend, different percentage of deformation were used, i.e., 50%, 100% and 150% (ϵ_m). The samples were heated at a temperature of 55 °C, for 5 min, and stretched until ϵ_m is reached by applying a constant deformation stress. They were then quenched at 0 °C under the same constant stress. The temporary shape was fixed after releasing the stress, and the permanent shape was recovered upon heating (3 °C/min) to 55 °C. Four different thermo-mechanical cycles have been performed for each material. Moreover, with the aim to get a quantitative estimation of the thermally-activated shape memory properties of the materials, the strain fixity ratio and the strain recovery ratio have been calculated. In particular, R_f , the ability to recover the initial shape, was taken as the ratio of the recovered strain to the total strain, as given by the following equation:

$$R_r(N) = \frac{(\epsilon_m - \epsilon_p(N))}{\epsilon_m - \epsilon_p(N-1)} \times 100 \% \quad (2)$$

R_f , the ability to fix the temporary shape, is the ratio of the fixed strain to the total strain, as presented by equation (3):

$$R_f(N) = \frac{\epsilon_u(N)}{\epsilon_m} \times 100 \% \quad (3)$$

where, ϵ_m is the deformed strain, ϵ_u the fixed strain, ϵ_p the recovered strain and N is the number of cycles. A qualitative study on the shape memory ability of the material at the different elongations was also carried out taken into account the strain energy involved in each cycle. The ideal strain energy was calculated as the integral of the whole curve obtained in the stress–strain diagrams thus considering an ideal behavior of the material where it is able to completely fix the temporary shape as well as to completely recover its original shape (R_f and $R_r = 100\%$). The real strain energy was taken as the integral of the curve obtained in the stress–strain diagrams taking in to account the real values of ϵ_u and ϵ_p obtained during each cycle. Thus, the energy efficiency has been calculated as the ratio between the real and the ideal strain energy [38].

The disintegration under composting conditions was carried out at laboratory scale level following the ISO 20200 standard [39]. Film samples (15 mm × 15 mm) were buried at 4–6 cm depth in

perforated plastic boxes containing a solid synthetic wet waste prepared with 10% of compost (Compo, Spain), 30% rabbit food, 10% starch, 5% sugar, 1% urea, 4% corn oil and 40% sawdust and about 50 wt % of water content and were incubated at aerobic conditions at 58 °C. Films were recovered at different disintegration times (7, 14, 28 and 42 days), washed with distilled water, dried in an oven (at 37 °C for 24 h) and reweighed to determine the degree of disintegrability by normalizing the sample weight at each time to the initial value. Moreover, a qualitative check of the visual appearance of films during disintegration in compost as a function of time was followed by taken photographs.

3. Results and discussion

3.1. Synthesis and functionalization of cellulose nanocrystals

The characterization of the pristine CNC and CNC-g-PLLA was previously reported in our work [35]. In brief, it was showed that rod-like shaped CNC of about 200 nm length and 20 nm diameter were successfully obtained by acid hydrolysis. The presence of PLLA chains grafted onto the CNC surface was demonstrated by FTIR and Raman spectroscopies and it lead to an increase of the average diameter, which was of about 25 nm [35].

Meanwhile, CNC functionalized by grafting PCL chains onto their surface were obtained and characterized in the present work. Three dispersions in chloroform, corresponding to a mixture of pristine CNC and PCL, pristine CNC and CNC-g-PCL are shown in Fig. 2. All of them were prepared with the same concentration for both CNC and PCL and were stirred for 2 h under magnetic stirring (Fig. 2 a). Fig. 2 b shows the mixtures after 48 h of stirring stop. The good dispersion obtained in chloroform for CNC-g-PCL demonstrated the success of the grafting reaction, as was previously reported also by Lannberg et al. [40].

The morphology of CNC-g-PCL was investigated by TEM as reported in Fig. 3, whereby they have the typical rod-like morphology. The average dimensions of PCL grafted CNC were

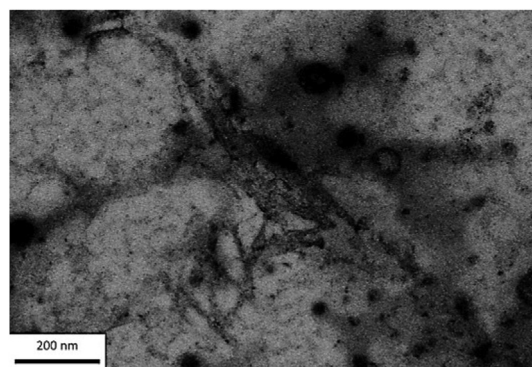


Fig. 3. TEM image of CNC-g-PCL nanofillers.

determined by image analysis with an average length of 163 ± 28 nm and a diameter of 18 ± 4 nm.

Vibrational spectroscopies were also used to characterize the CNC functionalization by grafting PCL chains onto their surface. In our case, FTIR and RAMAN spectroscopies were used as shown in Fig. 4. FTIR spectra of PCL, pristine CNC and CNC-g-PCL are reported in Fig. 4 a.

CNC-g-PCL spectrum shows both characteristic peaks of CNC and of PCL. For instance, the characteristic bands of hydroxyl of CNC in the region of 3200 cm^{-1} and 3600 cm^{-1} were observed in the CNC-g-PCL spectrum. Additionally, the band related with the carboxyl group of PCL at 1721 cm^{-1} reflects the presence of PCL onto the CNC surface, as it was previously reported by Habibi et al. [27].

The RAMAN spectra of PCL, pristine CNC and CNC-g-PCL are reported in Fig. 4 b. The characteristic bands of PCL were observed. The narrow peak at 1720 cm^{-1} was assigned to C=O stretching mode. Moreover, several further narrow peaks were observed at $1470\text{--}1415\text{ cm}^{-1}$ (CH_2 scissoring), $1303\text{--}1281\text{ cm}^{-1}$ (CH_2 wagging), $1107\text{--}1033\text{ cm}^{-1}$ (skeletal stretching) and 912 cm^{-1} (C–COO scissoring) [41]. Concerning CNC, the characteristic bands were observed in the Raman spectrum, such as the bands between 1200 and 1450 cm^{-1} due to C–C–H bending, CH_2 rocking and wagging, and C–O–H bending modes. The peaks in the region between 950 and 1150 cm^{-1} are originated from the skeletal ring stretches as well as the stretch modes of glycosidic C–O bonds and alcoholic C–O bonds. Below 950 cm^{-1} , the bending of skeletal C–C–C, C–O–C, O–C–C, and O–C–O bonds contributes [42]. The cellulose crystallinity can be also estimated from its vibration spectra. Indeed, the 380 cm^{-1} peak is observed only for crystalline cellulose and the 1095 cm^{-1} peak increased in intensity for higher crystalline cellulose [43]. Regarding the CNC-g-PCL spectrum, the characteristic bands of CNC and PCL were observed, confirming the FTIR

results.

The XRD analysis demonstrates that the grafted polymer chains can still crystallize, as it was previously reported for CNC-g-PLLA [35]. The grafted PCL chains were long enough to be able to crystallize at the surface of CNC [44]. The diffraction patterns of CNC-g-PCL shown the peaks related with the alpha form in the PCL crystalline phase, at 21.4° , 22.0° and 23.7° , and those of the cellulose ($2\theta = 14.8^\circ$, 16.5° , 22.6° and 34.5°) [27].

In order to quantify the amount of CNC and PCL in the CNC-g-PCL, TGA experiments were performed. The DTG curve for CNC-g-PCL is reported in Fig. 4 d, where two overlapped peaks ascribed to the thermal degradation of CNC and PCL chains, were observed. Contrary to CNC-g-PLLA [35], for CNC grafted with PCL chains, the first step of degradation was related to the CNC degradation, while the second one to the PCL chains degradation [45]. The estimation of the amount of each component was performed by fitting the curves with two Gaussian curves. The estimated amount of CNC and PCL on CNC-g-PCL was 70% of CNC and 30% of PCL, while for CNC-g-PLLA the estimated amount was previously found to be 57% and 43% for CNC and PLLA, respectively [35].

3.2. Characterization of CNC nanocomposites

PLA/PCL (70:30) blend and their nanocomposites reinforced with 1 wt % of CNC-based nanofillers either grafted or not with PLA or PCL chains, were prepared by melt-blending, and they were compression-molded at 180°C in order to obtain films of about 0.5 mm for their complete characterization. The visual aspect of obtained PLA/PCL blend (M70PLA) and its nanocomposites reinforced with 1 wt % of pristine CNC, CNC-g-PLLA and CNC-g-PCL nanofillers is shown in Fig. 5. From the visual appearance is possible to see that all nanocomposites resulted mostly transparent.

As it was previously demonstrated, adding small amount of

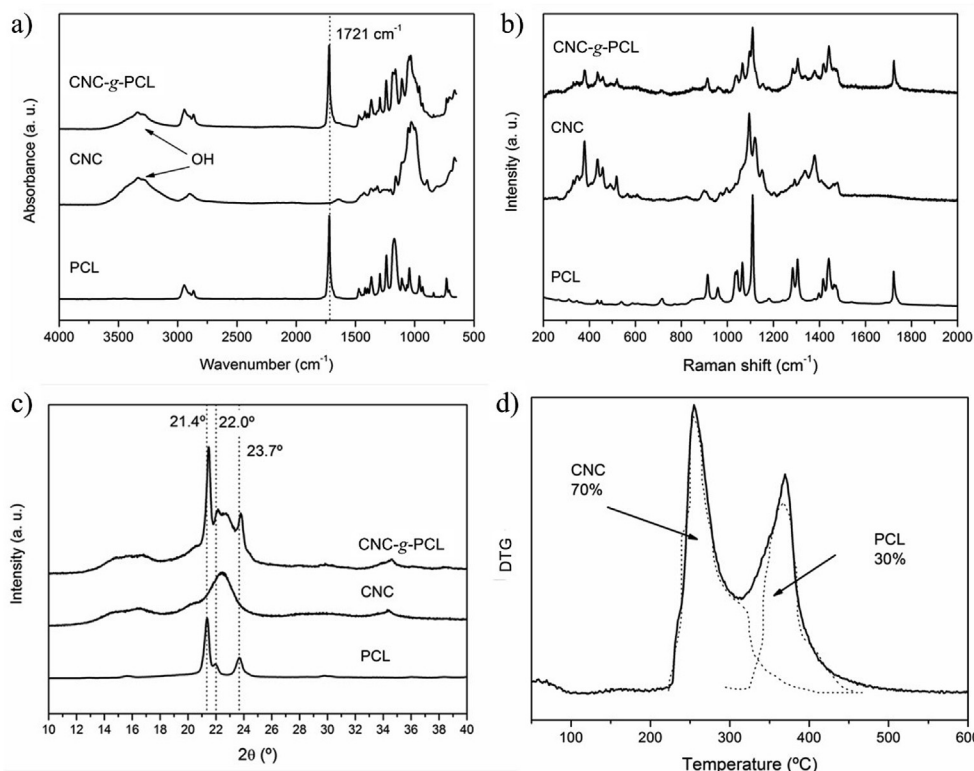


Fig. 4. Characterization of CNC-g-PCL: a) FTIR analysis, b) Raman spectroscopy, c) X-ray diffraction analysis and d) Thermogravimetric analysis.

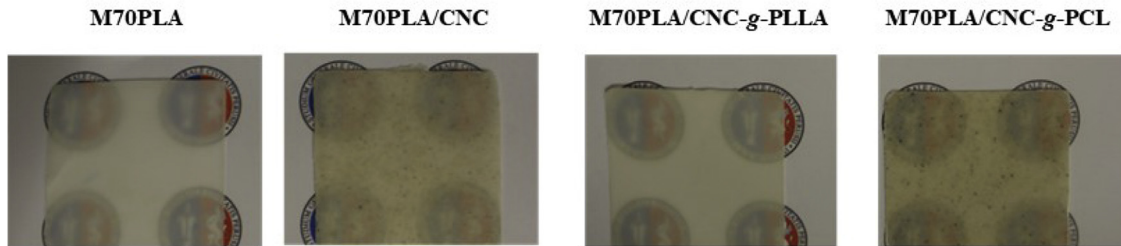


Fig. 5. Digital photographs of M70PLA-based nanocomposites reinforced with pristine and functionalized CNC nanofillers.

nanofillers is an effective way to manipulate the morphology of immiscible polymers [18,46]. The study of the nanocomposites morphology and compatibility is really important in order to understand the correlation among the degree of compatibility between both, PLA and PCL phase, and the thermally-activated shape memory ability [47].

The morphology of PCL/PLA nanocomposites reinforced with cellulose nanofillers was investigated by SEM analysis. The SEM images of the cryo-fractured surface of the nanocomposite reinforced with pristine CNC, CNC-g-PLLA and CNC-g-PCL are reported in Fig. 6. As it was reported in our previous work M70PLA shown typical “island” morphologies, where small PCL spheres are dispersed in the PLA matrix, indicating poor adhesion between both polymers, which confirms their immiscibility [8]. The SEM images of the nanocomposites show that the addition of CNC-based nanofillers strongly affect the morphology of the blend. During processing, the breakup of the dispersed PCL phase into smaller micro-domains is followed by a coalescent process while the

system tends to minimize its total free energy. Loading CNC-based nanofillers into this blend results in the migration of nanoparticles into the polymeric phase for which they show the stronger affinity and the lower interfacial tension, that is, in one of the two polymeric phases or at the interface between them. In particular, the nanoparticles located at the interface, stabilize the polymer phase morphology by decreasing the interfacial interactions as already reported in the literature [20]. In our case, M70PLA/CNC preserved the irregular “ellipsoid-like drop” distribution of PCL phase in the PLA matrix while M70PLA/CNC-g-PLLA and M70PLA/CNC-g-PCL showed a more spherical distribution of the PCL phase. Moreover, it is easy to notice out that the compatibility is also affected by the different types of functionalized nanofillers dispersed into the M70PLA blend matrix. In fact, using pristine CNC the PLA/PCL blend is characterized with a lacunar interface between both polymeric phases with the CNC located mainly in the PCL phase, while when using CNC-g-PLLA, the PCL phase not only changed their shape into more regular and smaller spheres with a maximum diameter of

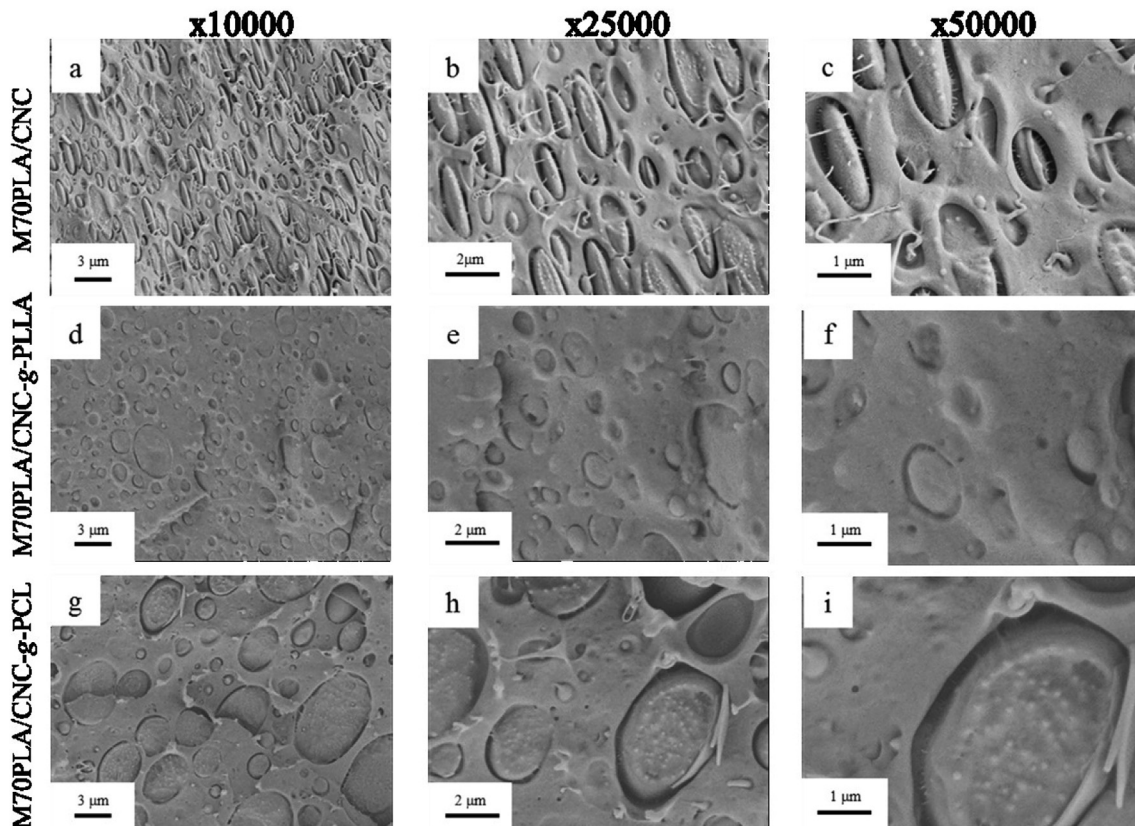


Fig. 6. SEM images of M70PLA nanocomposites with CNC nanofillers at different magnifications: M70PLA/CNC (a, b, c), M70PLA/CNC-g-PLLA (d, e, f) and M70PLA/CNC-g-PCL (g, h, i).

about 3 μm , but also the dimension of the lacunar interface was smaller or almost absent. This fact clearly shows that the compatibility between both phases, PLA and PCL, was increased by the addition of CNC-g-PLLA nanofillers, mainly located at their interface and acting as compatibilizer. On the other hand, when using the CNC-g-PCL nanofiller, the PCL spheres are bigger ($\approx 5 \mu\text{m}$) than those of M70PLA/CNC-g-PLLA and the dimension of the lacunar interface increased. Moreover, for M70PLA/CNC-g-PCL, the dispersed CNC-g-PCL can be observed mainly located into the PCL phase, confirming the good and selective interaction between these nanofillers and the PCL phase. From this analysis, it is possible to conclude that the morphology and the compatibility of the studied PLA/PCL blend can be controlled by the functionalization of the CNC-based nanofillers. In particular, these results suggested that the better compatibilization between both polymers, PLA and PCL, was reached by grafting PLLA chains onto the CNC surfaces.

The cellulose structures in the PLA/PCL blend matrix were also examined by FE-SEM (Fig. 7). In fact, CNC with dimensions ranging between 100 nm and 300 nm were identified in the cross section of the nanocomposite M70PLA/CNC (Fig. 7 a), confirming the effective incorporation of the synthesized nanocrystals into the PLA/PCL blend matrix. However, those CNC appears agglomerated. It was found that the size of the CNC was in agreement with the TEM observations previously reported in the literature [48]. More individualized nanocellulose structures can be distinguished from the FE-SEM images of M70PLA blend reinforced with CNC-g-PCL (Fig. 7 c) and particularly in the case of M70PLA/CNC-g-PLLA (Fig. 7 b), confirming the better dispersion of functionalized CNC.

Although the morphological observation is important to study the effect of the different CNC-based nanofillers on the thermally-activated shape memory behavior of PLA/PCL blend, both thermal and mechanical characterization are required in order to define the key-parameters for the shape memory analysis. At this regard, TGA and DSC analyses have been performed for their thermal characterization.

In Fig. 8 a, the TGA curves for all the samples are shown. As it was expected, the thermal degradation of the blend and its nanocomposites occurs in two steps ascribed to the PLA degradation first and then to the PCL degradation.

In our previous work [8], we studied the thermal stability of PLA, PCL as well as PLA/PCL blends at different proportions. Precisely, $T_{5\%}$ was found to be at 312 $^{\circ}\text{C}$ and 355 $^{\circ}\text{C}$ for PLA and PCL, respectively, while the maximum degradation temperature was found to be at 355 $^{\circ}\text{C}$ and 393 $^{\circ}\text{C}$ on the same order. For a better visualization of the degradation steps, the DTG curves are presented in Fig. 8 b and the main results are summarized in Table 1.

The $T_{5\%}$ and T_{max} of M70PLA were the same of neat PLA, indicating that the thermal stability of PLA did not change after the melt-blending process. Regarding the T_{max} of the nanocomposites, there was no difference comparing with the neat blend and its neat component. Meanwhile, the $T_{5\%}$ of the nanocomposites undergoes different changes depending on the CNC-based nanofillers added. In particular, the more significant variation was observed for

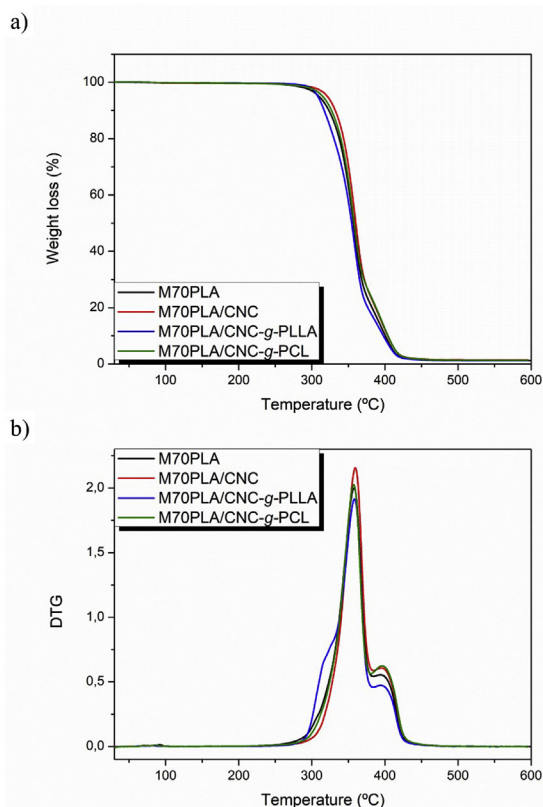


Fig. 8. TGA (a) and DTG (b) images for the M70PLA and its nanocomposites.

Table 1
TGA and DTG values of all the samples.

Sample	$T_{5\%}$ ($^{\circ}\text{C}$)	T_{max} PLA ($^{\circ}\text{C}$)	T_{max} PCL ($^{\circ}\text{C}$)
M70PLA	311	358	395
M70PLA/CNC	322	359	396
M70PLA/CNC-g-PLLA	309	358	395
M70PLA/CNC-g-PCL	316	357	397

M70PLA/CNC, which shows an increase of its $T_{5\%}$ of about 11 $^{\circ}\text{C}$. This fact is probably due to the good interaction between the fillers and the matrix where they are dispersed and it was already reported in literature for polyurethanes based on PLLA and PCL block copolymers filled with neat CNC [35] and for PLA/PHB/CNC ternary blend nanocomposites [48]. No important changes in the temperature corresponding to the initial degradation for the other nanocomposites were observed although they followed different trends. In fact, comparing with M70PLA, $T_{5\%}$ decreases a little (2 $^{\circ}\text{C}$) in the case of M70PLA/CNC-g-PLLA while it slightly increased for M70PLA/CNC-g-PCL (Table 1).

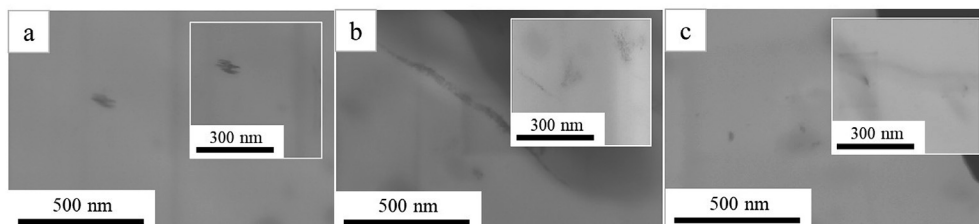


Fig. 7. FE-SEM images of nanocomposites at 100,000x (insert figure at 150,000x) of: a) M70PLA/CNC, b) M70PLA/CNC-g-PLLA and c) M70PLA/CNC-g-PCL.

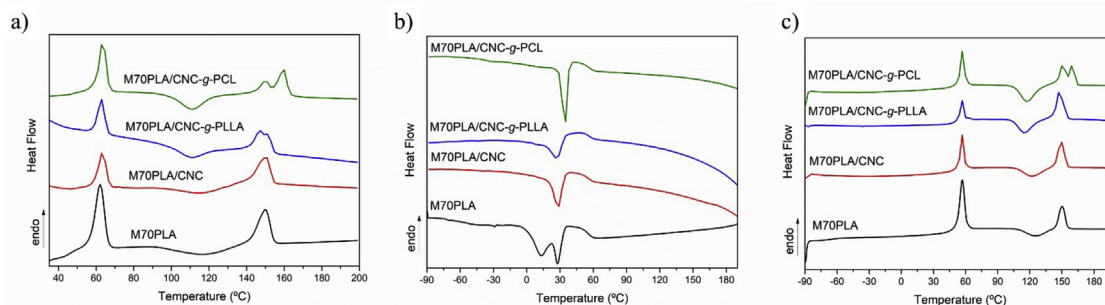


Fig. 9. DSC analyses for M70PLA and its nanocomposites with different CNC-based nanofillers. a) First heating scans, b) Cooling scans and c) second heating scans.

DSC measurements were performed to study the thermal properties and the melt/crystallization behavior of both PCL and PLA in the blend and its nanocomposites. In Fig. 9 the results for the thermal cycles (heating-cooling-heating) performed on all the materials are represented. The first heating (Fig. 9 a) shows the thermal properties of the blend as obtained after the processing, fundamental to determine the parameters for the shape memory cycles. No significant changes were observed between the first and the second heating scans. All the samples present the melting temperature of PCL around 60 °C and the melting peak of PLA at about 150 °C, all consistent with literature values.

In our previous work [8], the T_g and T_m of neat PLA was found to be around 60 °C and 150 °C, respectively while those of PCL were of –63 and 58 °C, respectively. T_m of both PCL and PLA homopolymers are not strongly affected neither in the blend nor in the nanocomposites. It is worth noting that for the blend and the nanocomposites was difficult to determine the T_g of both polymers during the heating scans, namely for PLA due to its overlapping with the melting peak of PCL. For this reason, the T_g values of PLA, for the blend and its nanocomposites, were taken from the cooling scan as a reference. The main results taken from the second heating scan of DSC analysis are summarized in Table 2. The T_c and the T_g of both components were taken from the cooling scan. The T_g of PCL slightly increase in M70PLA/CNC-g-PLLA, indicating that the addition of functionalized CNC decreases the PCL chains mobility as already reported in literature [35]. Moreover, the degree of crystallinity of PCL decreased for the nanocomposites depending on the CNC-based filler. Using pristine CNC and functionalized CNC (CNC-g-PCL and CNC-g-PLLA), the degree of crystallinity slightly decreases, reaching the minimum value for M70PLA/CNC-g-PLLA where probably CNC-g-PLLA can hinder the reorganization of PCL chains for crystallizing, confirming the decrease of the PCL chains mobility. On the contrary, for M70PLA/CNC-g-PCL an increase of the crystallization temperature was observed, indicating that CNC-g-PCL can facilitate the crystallization of PCL during the cooling process.

As it is possible to notice in Fig. 9 a, the cold crystallization of PLA is also observed in the first heating scan, indicating that the PLA did not reach the fully degree of crystallinity during the

compression molding cooling, although for the nanocomposites reinforced with functionalized CNC, this fact is much more visible. Furthermore, in the first heating scan the presence of two melting peaks located between 147/151 °C for M70PLA/CNC-g-PLLA and 150/159 °C for M70PLA/CNC-g-PCL was observed. These observations indicate that functionalized CNC in PLA matrix can act as nucleation agent and they can modify the PLA crystal growth. This affects the phase behavior such as the interfacial adhesion between both polymers and consequently the miscibility of the blend, as already reported [18].

The mechanical properties were studied through stress-strain experiments. In Fig. 10, the obtained results in terms of elastic modulus, tensile strength and elongation at break of all the processed materials are reported. The nanocomposites show higher elastic modulus (Fig. 10 a) as well as tensile strength (Fig. 10 b), reaching the highest values for M70PLA/CNC-g-PLLA. This indicates the good effect of the functionalization on the dispersion of the nanofillers into the polymeric matrix. Regarding the elongation at break, the nanocomposite reinforced with CNC-g-PLLA shown the highest value by comparing with the neat blend as it is showed in Fig. 10 c. In fact, reinforcing M70PLA with pristine CNC and CNC-g-PCL a dramatic decrease of the elongation at break is provoked. These results suggest that better compatibilization between both polymers, PLA and PCL, was reached by grafting PLLA chains onto the CNC surfaces, as it was previously commented for SEM and FE-SEM results.

Furthermore, once studied the morphological, thermal and mechanical properties of the nanocomposites compared to that of the neat blend, it is easier to fix the parameters to perform the thermally-activated shape memory analysis. In particular, as it was previously described, thermo-mechanical cycles were performed by DMTA at a T_{sw} near to the T_m of PCL in our system, while PLA acts as permanent phase. The digital photographs reported on Fig. 11 correspond to M70PLA/CNC-g-PLLA, as example of the visual appearance of the thermally-activated shape memory process. As it is worth noting, the sample at room temperature is white-colored mostly because of the crystalline phase of PCL. In fact, when the sample were heated at the selected $T_{sw} = 55$ °C, it became almost totally transparent. Like the corresponding thermo-mechanical

Table 2
Thermal properties of M70PLA and its nanocomposites.

Sample	PCL				PLA			
	T_m (°C)	T_c (°C)	X_c (%)	T_g (°C)	T_m (°C)	T_c (°C)	X_c (%)	T_g (°C)
M70PLA	57	28	34	–64	150	–	3	55
M70PLA + 1% CNC	57	29	26	–	150	–	2	54
M70PLA + 1% CNC-g-PLLA	57	26	17	–43	147	–	1	56
M70PLA + 1% CNC-g-PCL	57	35	30	–	150	–	1	56

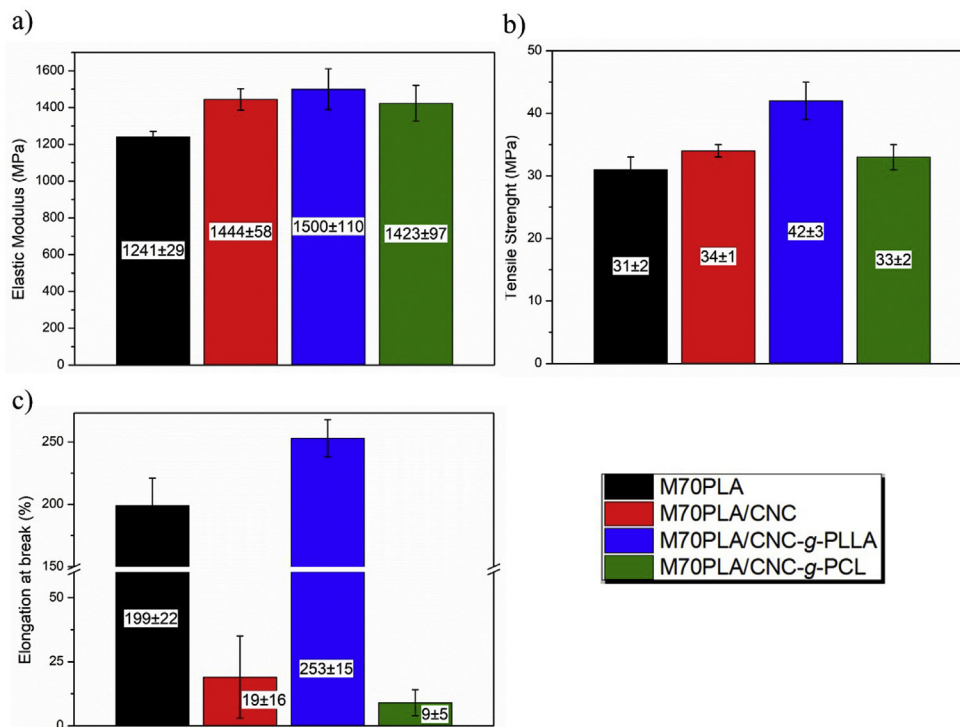


Fig. 10. Mechanical properties of PLA/PCL blend and the CNC-based nanocomposites.

cycles constructed upon different stages, the sample was first heated at 55 °C and folded (Fig. 11.2). Then, it was cooled down by fixing the temporary shape reported in Fig. 11.3. Heating again at 55 °C (Figs. 11.4–5–6), the crystalline phase of PCL melts and the sample can recover their initial shape as it is clearly shown in the photograph sequences of Fig. 11.

The thermo-mechanical cycles were performed at different elongations, such as 50%, 100% and 150%. The programming step was designed with a uniaxial stretching at 55 °C, followed by a fast quenching of the stretched state at 0 °C. The stretched state was maintained after quenching and subsequent removal of the stress at 0 °C. Fig. 12 presents the evolution of strain, stress, and temperature in function of time during the dual-shape memory programming step and the 3D stress-strain-temperature diagrams for MPLA/CNC at different percentage of deformation, as example. The thermo-mechanical cycles diagrams performed using the same

parameters for M70PLA, M70PLA/CNC-g-PLLA and M70PLA/CNC-g-PCL are reported in Supporting Information. It is worth noting that all the samples showed an increase of the applied stress increasing the number of cycles probably due to the crystallization of the blend. This fact suggests that the samples probably underwent a crystallization phenomenon due to the annealing process at T_{sw} during the recovery stage of the thermo-mechanical cycle. The effect of annealing process on the properties of PLA/PCL was already reported in literature [49], showing that the crystallization of the PLA phase after annealing strengthens the structure of the PLA/PCL blend, resulting in the increase of mechanical properties. For the sample with better compatibility and with the highest mechanical properties (M70PLA/CNC-g-PLLA), the thermo-mechanical cycle was interrupted at the cycle 2 because the maximum distance between the DMTA clamps was reached during the deformation step of the cycle 3. On the other hand, all the samples shown good ability to fix the deformed shape until the selected T_{sw} as it is well visible in the diagrams reported in Fig. 12 confirming the perfect control of the shape memory performance of the materials.

In Table 3, the results of thermomechanical cycles in terms of R_f and R_r are summarized for the different percentage of deformation. As it is possible to note, the blend and its nanocomposites show excellent shape memory properties reaching values higher than 80% and 98% for R_r and R_f respectively.

The analysis of the strain energy involved in the shape memory experiments for the blend and its nanocomposites was carried out following the same procedure reported previously [38]. The strain energy of an ideal shape memory polymer was estimated taking into account that the fixed shape should be perfectly equal to the deformed shape and that an ideal material is able to recover all the applied deformation. Thus, the ideal (ISE) as well as the real strain energy (RSE) of the nanocomposites were calculated in this work for all the sample at the different percentage of elongation. A comparison of the strain energy obtained during the different cycles for all the samples is shown in Fig. 13. As it was expected,

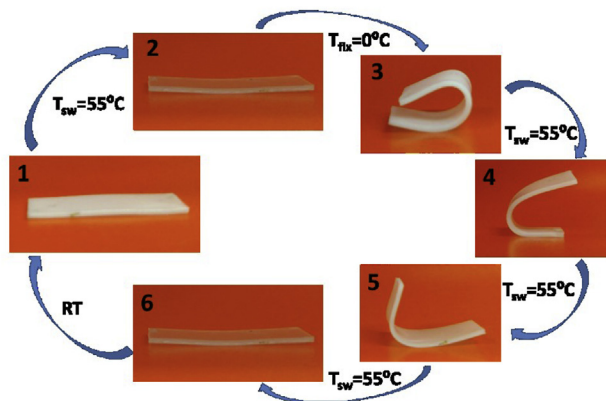


Fig. 11. Scheme of the shape memory mechanism used for M70PLA and its nanocomposites.

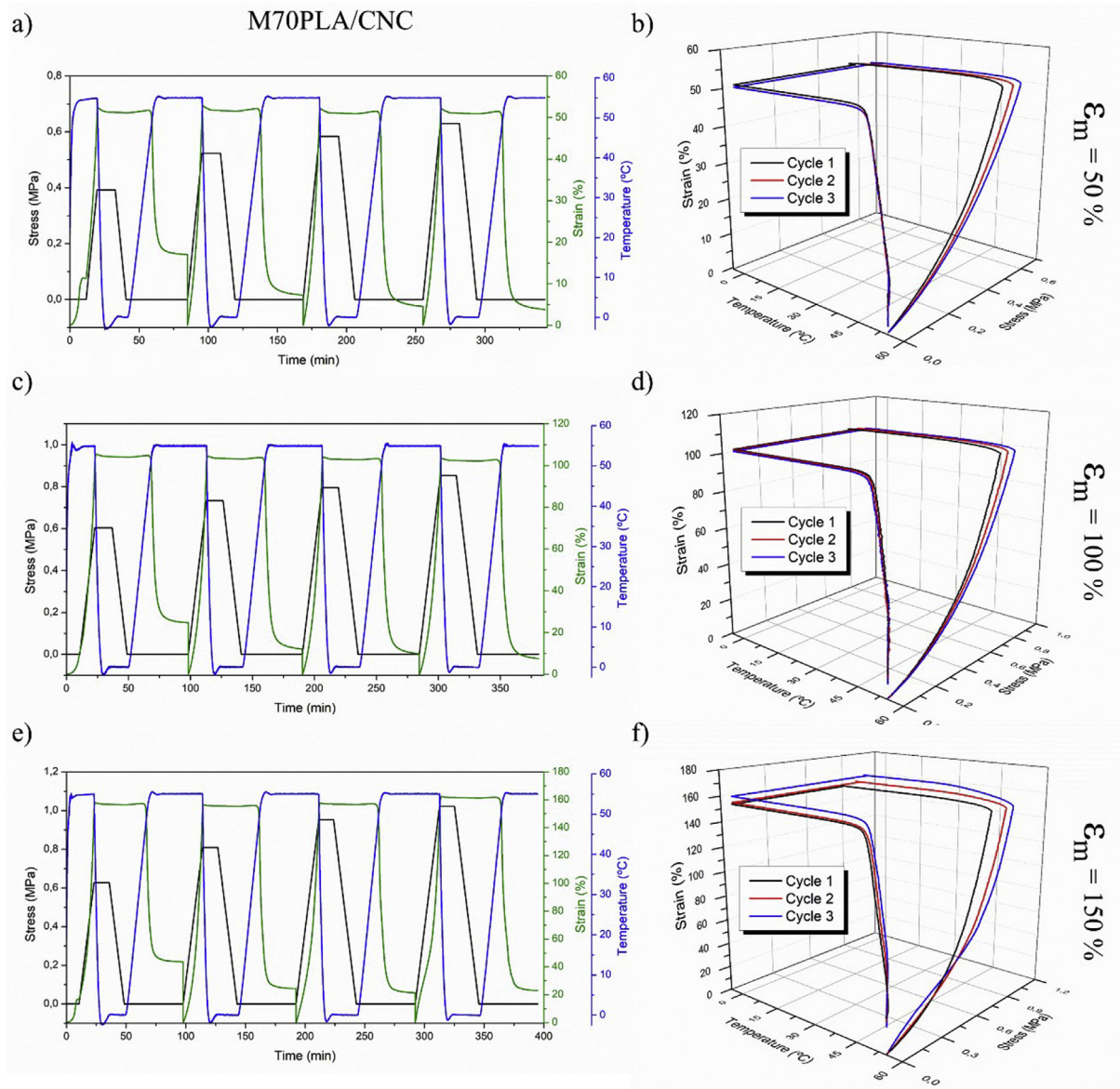


Fig. 12. Evolution of stress strain and temperature in function of time and 3D stress-strain-temperature, respectively for: a-b) 50% of deformed strain, c-d) 100% deformed strain and e-f) 150% deformed strain.

Table 3

R_r and R_f and Energy Efficiency values for all the sample tested at different percentage of elongation during the thermo-mechanical cycles.

Sample	ϵ_m (%)	R_r (%)			R_f (%)			Energy Efficiency (%)		
		1	2	3	1	2	3	1	2	3
M70PLA	50	92	95	95	99	99	99	97.6	98.6	99.6
	100	88	89	88	99	99	99	96.8	96.9	96.6
	150	87	87	87	99	99	99	95.8	96.2	97.6
M70PLA/CNC	50	86	91	93	98	98	98	96.5	98.3	99.5
	100	88	91	93	99	99	99	96.8	97.7	98.5
	150	84	86	86	99	99	99	94.3	96.4	97.9
M70PLA/CNC-g-PLLA	50	85	89	82	98	98	98	95.6	97.3	99.4
	100	89	90	93	99	99	99	97.3	97.6	98.5
	150	82	81	—	99	99	—	98.5	93.5	—
M70PLA/CNC-g-PCL	50	87	93	87	98	98	98	97.0	98.7	96.4
	100	86	87	88	99	99	99	95.6	96.3	97.1
	150	88	88	86	99	99	99	96.2	97.8	98.0

increasing the percentage of elongation, the strain energy involved is higher. Comparing with the other nanocomposites and the blend, M70PLA/CNC-g-PLLA shows the higher values of strain energy at 150% of deformation suggesting that probably the effect of the annealing process was higher for the nanocomposite reinforced with CNC-g-PLLA which probably induced the crystallization most in the interface of the phases leading to an increase of the compatibility, as it was previously reported [18]. The energy efficiency for all cycles, as the ratio between the real and the ideal energies was calculated for all the samples and the values are summarized in Table 3. For all the materials, the energy efficiency is very high indicating that the reinforcing effect of CNC-based nanofillers on the blend did not affect the shape memory performances.

These results suggested that shape memory ability of nanocomposites based on immiscible blend such as PLA/PCL is mainly

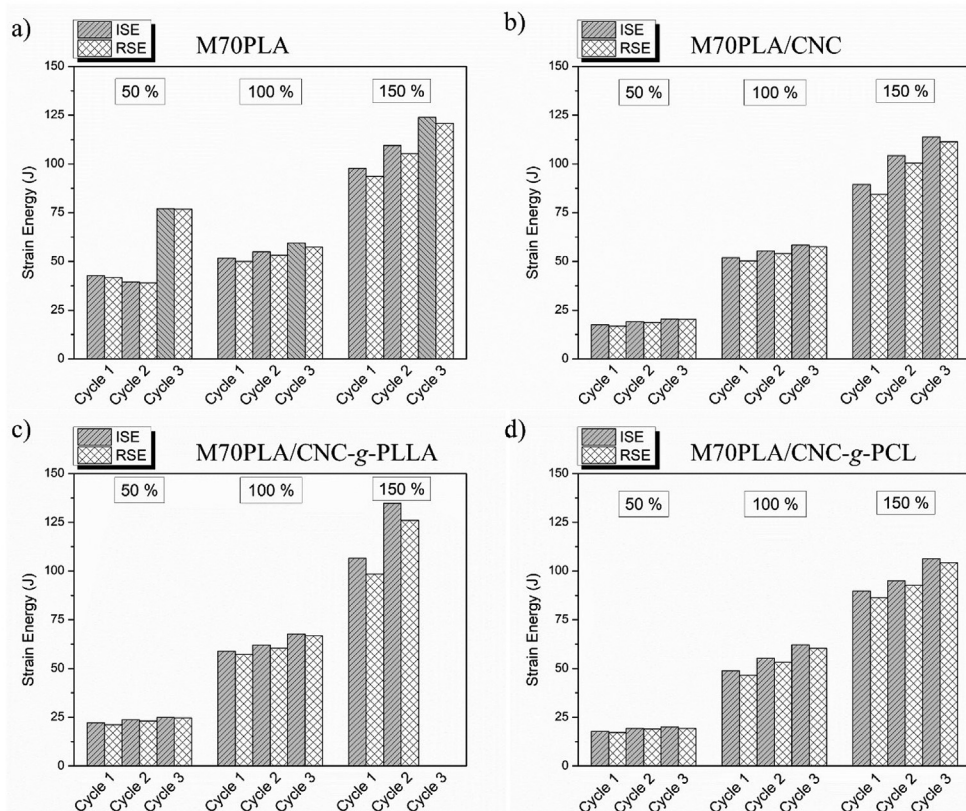


Fig. 13. Comparison of ideal and real strain energy at different percentage of elongation for all the sample during the thermo-mechanical cycles; a) M70PLA, b) M70PLA/CNC, c) M70PLA/CNC-g-PLLA and d) M70PLA/CNC-g-PCL.

controlled by the response of the neat materials. In fact, although different morphology and mechanical properties were observed using different CNC-based nanofillers, no evident changes on the shape memory response of the nanocomposites were observed, thus considering that in this case their shape memory capability is strongly driven by the response of the polymeric matrix itself. Shape memory performances was slightly influenced by the increase of compatibility between the components of the blend and was not affected by the reinforcing effect of CNC-based nanofillers. These results are very important, thus considering that in our previous work based on polyurethane reinforced with CNC [38] it was not possible to study the shape memory response of the neat matrix and of its nanocomposites at the same transition temperature, due to a change in the crystalline phase of the PCL block. However, in this case, the shape memory response of both neat matrix and nanocomposites can be study at the same transition temperature, 55 °C.

Finally, in order to study how the CNC-based nanofillers can affect the degradation properties of the PLA/PCL blend, the disintegrability of all the samples under composting conditions, was tested. The visual appearance of recovered films at different composting times is shown in <http://www.sciencedirect.com/science/article/pii/S0926669017307276> Fig. 14 a, while the corresponding mass loss as a function of time is showed in <http://www.sciencedirect.com/science/article/pii/S0926669017307276> Fig. 14 b.

During the first week of composting M70PLA-based nanocomposites and particularly neat M70PLA lost their transparency. The materials experimented a change in the refraction index as a result of water absorption and/or because of the hydrolytic degradation process was taking place [50,51]. Most of materials became breakable at this stage, whit the exception of M70PLA/CNC-g-PLLA

that was the most flexible material, as it was discussed in tensile test results. Moreover, at 14 days this sample reached the highest disintegrability (losing 24% of its initial weight). This behavior is due to the increased polymer chain mobility, which allowed higher hydrolysis leading to a reduction of the molecular weight and the small molecules (i.e. monomers and short-chain oligomers) being more available for the microorganisms attack [52,53]. In fact, the more flexible the material, the greater the weight loss and this tendency continued up to 21 days. At 28 days, samples were broken into small dark-brown pieces and all of them reached above 50% of disintegration. At 42 days films became almost black and all nanocomposites reached the goal of disintegrability test (more than 90% of weight loss) being M70PLA/CNC-g-PLLA the most disintegrated samples again. The hydrophilic nature of CNC and functionalized CNC speeded up the disintegration rate of the nanocomposites, in good agreement with previously results [6]. Finally, in 55 days M70PLA was completely disintegrated.

4. Conclusions

A deep study about the effect of the addition of CNC-based nanofillers on the thermally-activated shape memory response of the blend and its nanocomposites was conducted in this work. In particular, the effect of the addition of 1 wt % of cellulose nanocrystals-based nanofillers in a PLA/PCL blend was studied pointed out their morphological, thermal and mechanical properties. Cellulose nanocrystals were subjected to different chemical modifications leading to the grafting of PLLA and PCL chains onto their surface. The study revealed that the compatibilization of the PLA/PCL blend was affected by the addition of the different CNC-based nanofillers. The affinity between the functionalized CNC

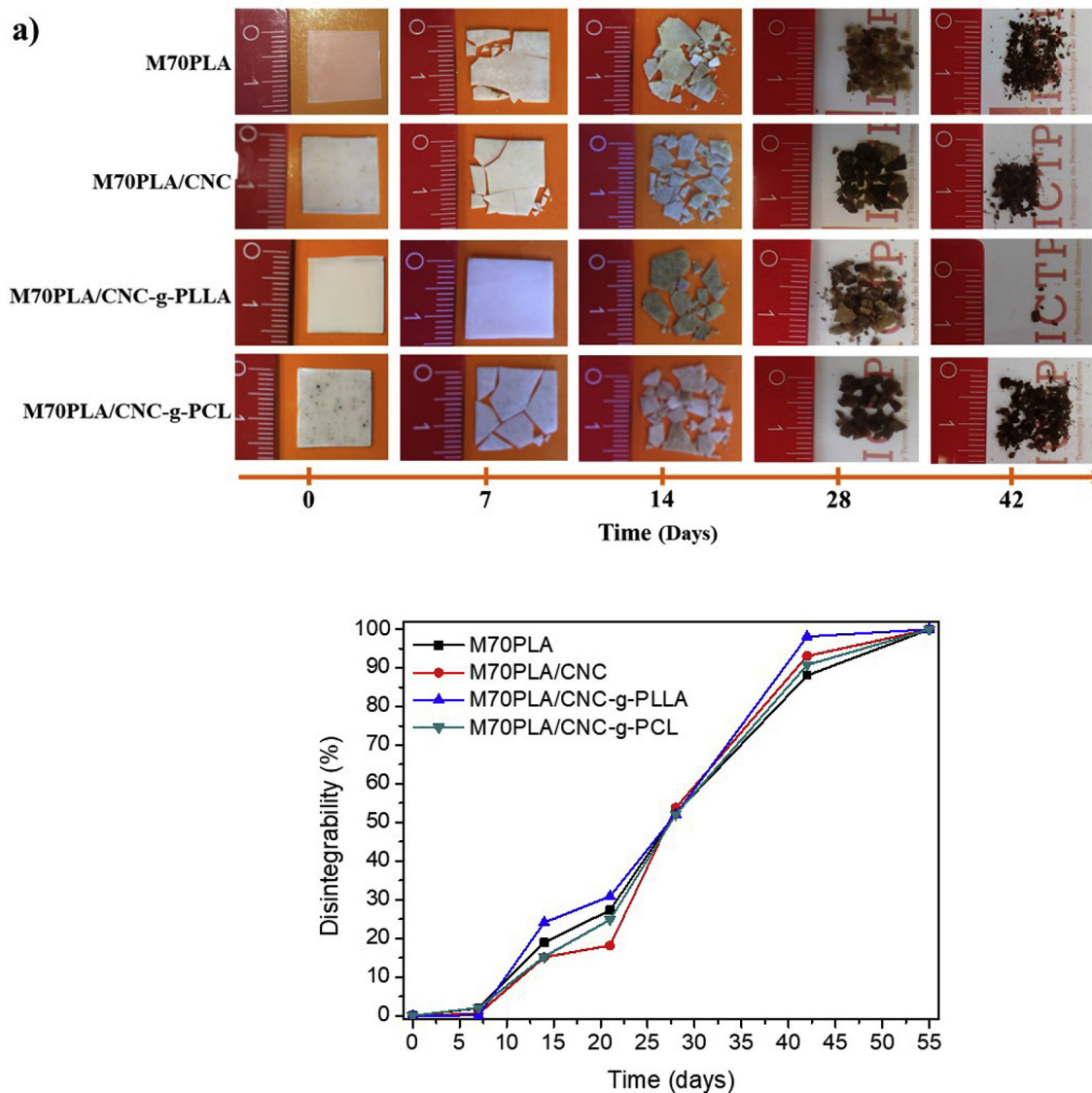


Fig. 14. Disintegrability under composting condition of PLA/PCL blend and its nanocomposites. a) Visual appearance of disintegrated specimens and b) disintegrability as a function of time.

and the blend components determine their localization. Better interfacial adhesion was obtained by the incorporation of CNC-g-PLLA into the blend matrix, probably due to the localization of the nanofiller mainly in the blend interface. This fact was confirmed by the improvement of the mechanical properties mostly for M70PLA/CNC-g-PLLA, which showed an increase of all the measured parameters such as, elastic modulus, tensile strength and the elongation at break. On the other hand, for the shape memory properties was found that they are mainly controlled by the response of the neat blend and they are slightly influenced by the increase of compatibility between the components of the blend. In fact, comparing with the neat matrix, at the same transition temperature, the thermally-activated shape memory response of the nanocomposites was not affected by the addition of CNC-based nanofillers, presenting excellent values for both strain recovery ratio and strain fixity ratio, higher than 80% and 98%, respectively. Moreover, it was found that the samples probably underwent a crystallization phenomenon due to the annealing process at T_{sw} during the recovery stage of the thermo-mechanical cycle. Additionally, the disintegrability test confirmed the biodegradable

character of these nanocomposites that can be useful in different areas such as biomedicine or food packaging.

Acknowledgements

Authors thank the Spanish Ministry of Economy, Industry and Competitiveness (MINEICO) (MAT2017-88123-P), POLYMAGIC: (PCIN-2017-036) cofinanced with FEDER funds and the Regional Government of Madrid (S2013/MIT-2862). M.P.A. and L.P. acknowledge the “Juan de la Cierva” (FJCI-2014-20630) and “Ramon y Cajal” (RYC-2014-15595) contracts from the MINEICO, respectively. The authors also thank CSIC for the I-Link project (I-Link1149). JMR is a FRS-FNRS research associate.

Appendix A. Supplementary data

Supplementary data related to this article can be found at <https://doi.org/10.1016/j.polymdegradstab.2018.04.012>.

References

- [1] M. Arrieta, L. Peponi, D. López, M. Fernández-García, Recovery of yerba mate (*Ilex paraguariensis*) residue for the development of PLA-based bionanocomposite films, *Ind. Crop. Prod.* 111 (2018) 317–328.
- [2] G.E. Luckachan, C. Pillai, Biodegradable polymers—a review on recent trends and emerging perspectives, *J. Polym. Environ.* 19 (2011) 637–676.
- [3] L. Peponi, D. Puglia, L. Torre, L. Valentini, J.M. Kenny, Processing of nanostructured polymers and advanced polymeric based nanocomposites, *Mater. Sci. Eng. R Rep.* 85 (2014) 1–46.
- [4] N. Burgos, D. Tolaguera, S. Fiori, A. Jiménez, Synthesis and characterization of lactic acid oligomers: evaluation of performance as poly (lactic acid) plasticizers, *J. Polym. Environ.* 22 (2014) 227–235.
- [5] F. Hassouna, J.-M. Raquez, F. Addiego, P. Dubois, V. Toniazzo, D. Ruch, New approach on the development of plasticized polylactide (PLA): grafting of poly (ethylene glycol)(PEG) via reactive extrusion, *Eur. Polym. J.* 47 (2011) 2134–2144.
- [6] M. Arrieta, E. Fortunati, F. Dominici, J. López, J. Kenny, Bionanocomposite films based on plasticized PLA-PHB/cellulose nanocrystal blends, *Carbohydr. Polym.* 121 (2015) 265–275.
- [7] J. Ferri, D. Garcia-García, L. Sánchez-Nacher, O. Fenollar, R. Balart, The effect of maleinized linseed oil (MLO) on mechanical performance of poly (lactic acid)-thermoplastic starch (PLA-TPS) blends, *Carbohydr. Polym.* 147 (2016) 60–68.
- [8] I. Navarro-Baena, V. Sessini, F. Dominici, L. Torre, J.M. Kenny, L. Peponi, Design of biodegradable blends based on PLA and PCL: from morphological, thermal and mechanical studies to shape memory behavior, *Polym. Degrad. Stabil.* 132 (2016) 97–108.
- [9] R.V. Castillo, A.J. Muller, J.-M. Raquez, P. Dubois, Crystallization kinetics and morphology of biodegradable double crystalline PLLA-b-PCL diblock copolymers, *Macromolecules* 43 (2010) 4149–4160.
- [10] I. Navarro-Baena, M.P. Arrieta, A. Sonseca, L. Torre, D. López, E. Giménez, et al., Biodegradable nanocomposites based on poly (ester-urethane) and nanosized hydroxyapatite: plasticizer and reinforcement effects, *Polym. Degrad. Stabil.* 121 (2015) 171–179.
- [11] M. Arrieta, E. Fortunati, F. Dominici, E. Rayón, J. López, J. Kenny, PLA-PHB/cellulose based films: mechanical, barrier and disintegration properties, *Polym. Degrad. Stabil.* 107 (2014) 139–149.
- [12] J. Odent, Y. Habibi, J.-M. Raquez, P. Dubois, Ultra-tough polylactide-based materials synergistically designed in the presence of rubbery ϵ -caprolactone-based copolyester and silica nanoparticles, *Compos. Sci. Technol.* 84 (2013) 86–91.
- [13] D. Wu, Y. Zhang, M. Zhang, W. Yu, Selective localization of multiwalled carbon nanotubes in poly (ϵ -caprolactone)/polylactide blend, *Biomacromolecules* 10 (2009) 417–424.
- [14] W.H. Hoidy, E.A.J. Al-Mulla, K.W. Al-Janabi, Mechanical and thermal properties of PLLA/PCL modified clay nanocomposites, *J. Polym. Environ.* 18 (2010) 608–616.
- [15] K. Fukushima, D. Tabuani, C. Abbate, M. Arena, L. Ferreri, Effect of sepiolite on the biodegradation of poly (lactic acid) and polycaprolactone, *Polym. Degrad. Stabil.* 95 (2010) 2049–2056.
- [16] K. Fukushima, D. Tabuani, G. Camino, Nanocomposites of PLA and PCL based on montmorillonite and sepiolite, *Mater. Sci. Eng. C* 29 (2009) 1433–1441.
- [17] S. Jain, M.M. Reddy, A.K. Mohanty, M. Misra, A.K. Ghosh, A new biodegradable flexible composite sheet from poly (lactic acid)/poly (ϵ -caprolactone) blends and Micro-Talc, *Macromol. Mater. Eng.* 295 (2010) 750–762.
- [18] A.-L. Goffin, Y. Habibi, J.-M. Raquez, P. Dubois, Polyester-grafted cellulose nanowhiskers: a new approach for tuning the microstructure of immiscible polyester blends, *ACS Appl. Mater. Interfaces* 4 (2012) 3364–3371.
- [19] J. Yu, F. Ai, A. Dufresne, S. Gao, J. Huang, P.R. Chang, Structure mechanical properties of Poly (lactic acid) Filled with (Starch nanocrystal)-graft-poly (ϵ -caprolactone), *Macromol. Mater. Eng.* 293 (2008) 763–770.
- [20] J. Odent, J.-M. Raquez, J.-M. Thomassin, J.-M. Gloguen, F. Lauro, C. Jérôme, et al., Mechanistic insights on nanosilica self-networking inducing ultra-toughness of rubber-modified polylactide-based materials, *Nanocomposites* 1 (2015) 113–125.
- [21] E. Fortunati, I. Armentano, Q. Zhou, A. Iannoni, E. Saino, L. Visai, et al., Multifunctional bionanocomposite films of poly (lactic acid), cellulose nanocrystals and silver nanoparticles, *Carbohydr. Polym.* 87 (2012) 1596–1605.
- [22] N. Herrera, A.P. Mathew, K. Oksman, Plasticized polylactic acid/cellulose nanocomposites prepared using melt-extrusion and liquid feeding: mechanical, thermal and optical properties, *Compos. Sci. Technol.* 106 (2015) 149–155.
- [23] J.K. Muiruri, S. Liu, W.S. Teo, J. Kong, C. He, Highly biodegradable and tough polylactic acid–cellulose nanocrystal composite, *ACS Sustain. Chem. Eng.* 5 (2017) 3929–3937.
- [24] G. Siqueira, J. Bras, N. Follain, S. Belbekhouche, S. Marais, A. Dufresne, Thermal and mechanical properties of bio-nanocomposites reinforced by Luffa cylindrical cellulose nanocrystals, *Carbohydr. Polym.* 91 (2013) 711–717.
- [25] A.-L. Goffin, J.-M. Raquez, E. Duquesne, G. Siqueira, Y. Habibi, A. Dufresne, et al., From interfacial ring-opening polymerization to melt processing of cellulose nanowhisker-filled polylactide-based nanocomposites, *Biomacromolecules* 12 (2011) 2456–2465.
- [26] N. Lin, G. Chen, J. Huang, A. Dufresne, P.R. Chang, Effects of polymer-grafted natural nanocrystals on the structure and mechanical properties of poly(lactic acid): a case of cellulose whisker-graft-polycaprolactone, *J. Appl. Polym. Sci.* 113 (2009) 3417–3425.
- [27] Y. Habibi, A.-L. Goffin, N. Schiltz, E. Duquesne, P. Dubois, A. Dufresne, Bionanocomposites based on poly (ϵ -caprolactone)-grafted cellulose nanocrystals by ring-opening polymerization, *J. Mater. Chem.* 18 (2008) 5002–5010.
- [28] J. Odent, J.-M. Raquez, C. Samuel, S. Barrau, A. Enotiadis, P. Dubois, et al., Shape-memory behavior of polylactide/silica ionic hybrids, *Macromolecules* 50 (2017) 2896–2905.
- [29] V. Sessini, M.P. Arrieta, A. Fernández-Torres, L. Peponi, Humidity-activated shape memory effect on plasticized starch-based biomaterials, *Carbohydr. Polym.* 179 (2018) 93–99.
- [30] V. Sessini, J.-M. Raquez, G. Lo Re, R. Mincheva, J.M. Kenny, P. Dubois, et al., Multiresponsive shape memory blends and nanocomposites based on starch, *ACS Appl. Mater. Interfaces* 8 (2016) 19197–19201.
- [31] A.S. Olalla, V. Sessini, E.G. Torres, L. Peponi, Smart nanocellulose composites with shape-memory behavior, in: D. Puglia, E. Fortunati, J.M. Kenny (Eds.), *Multifunctional Polymeric Nanocomposites Based on Cellulosic Reinforcements*, Elsevier, 2016, pp. 277–312.
- [32] E.D. Cranston, D.G. Gray, Morphological and optical characterization of polyelectrolyte multilayers incorporating nanocrystalline cellulose, *Biomacromolecules* 7 (2006) 2522–2530.
- [33] N. Bitinis, R. Verdejo, J. Bras, E. Fortunati, J.M. Kenny, L. Torre, et al., Poly(lactic acid)/natural rubber/cellulose nanocrystal bionanocomposites Part I. Processing and morphology, *Carbohydr. Polym.* 96 (2013) 611–620.
- [34] O. Paquet, M. Krouit, J. Bras, W. Thielemans, M.N. Belgacem, Surface modification of cellulose by PCL grafts, *Acta Mater.* 58 (2010) 792–801.
- [35] I. Navarro-Baena, J. Kenny, L. Peponi, Thermally-activated shape memory behaviour of bionanocomposites reinforced with cellulose nanocrystals, *Cellulose* 21 (2014) 4231–4246.
- [36] L. Peponi, I. Navarro-Baena, J.E. Báez, J.M. Kenny, A. Marcos-Fernández, Effect of the molecular weight on the crystallinity of PCL-b-PLLA di-block copolymers, *Polymer* 53 (2012) 4561–4568.
- [37] I. Standard, B. ISO, Rubber, Vulcanized or Thermoplastic—Determination of Tensile Stress-strain Properties, International Organization for Standardization, Geneva, 2005.
- [38] L. Peponi, I. Navarro-Baena, A. Sonseca, E. Gimenez, A. Marcos-Fernandez, J.M. Kenny, Synthesis and characterization of PCL–PLLA polyurethane with shape memory behavior, *Eur. Polym. J.* 49 (2013) 893–903.
- [39] U.-E. Plastics, Determination of the Degree of Disintegration of Plastic Materials under Simulated Composting Conditions in a Laboratory-scale Test (ISO20200:2015), 2016.
- [40] H. Lönnberg, L. Fogelström, L. Berglund, E. Malmström, A. Hult, M.A.S.A. Samir, Surface grafting of microfibrillated cellulose with poly (ϵ -caprolactone)—Synthesis and characterization, *Eur. Polym. J.* 44 (2008) 2991–2997.
- [41] G. Kister, G. Cassanas, M. Bergounhon, D. Hoarau, M. Vert, Structural characterization and hydrolytic degradation of solid copolymers of d,l-lactide-co- ϵ -caprolactone by Raman spectroscopy, *Polymer* 41 (2000) 925–932.
- [42] S.H. Kim, C.M. Lee, K. Kafle, Characterization of crystalline cellulose in biomass: basic principles, applications, and limitations of XRD, NMR, IR, Raman, and SFG, *Kor. J. Chem. Eng.* 30 (2013) 2127–2141.
- [43] U.P. Agarwal, Raman Spectroscopy of CNC- and CNF-based Nanocomposites, *Handbook of Nanocellulose and Cellulose Nanocomposites*, 2017, pp. 609–625.
- [44] Y. Habibi, Key advances in the chemical modification of nanocelluloses, *Chem. Soc. Rev.* 43 (2014) 1519–1542.
- [45] C. Tian, S. Fu, J. Chen, Q. Meng, L.A. Lucia, Graft polymerization of epsilon-caprolactone to cellulose nanocrystals and optimization of grafting conditions utilizing a response surface methodology, *Nord. Pulp Pap Res. J.* 29 (2014) 58–68.
- [46] M.S. de Luna, G. Filippone, Effects of nanoparticles on the morphology of immiscible polymer blends—challenges and opportunities, *Eur. Polym. J.* 79 (2016) 198–218.
- [47] V. Sessini, J.-M. Raquez, D. Lourdin, J.-E. Maigret, J.M. Kenny, P. Dubois, et al., Humidity-activated shape memory effects on thermoplastic starch/EVA blends and their compatibilized nanocomposites, *Macromol. Chem. Phys.* 218 (2017), 1700388-n/a.
- [48] M. Arrieta, E. Fortunati, F. Dominici, E. Rayón, J. López, J. Kenny, Multifunctional PLA–PHB/cellulose nanocrystal films: processing, structural and thermal properties, *Carbohydr. Polym.* 107 (2014) 16–24.
- [49] T. Takayama, M. Todo, H. Tsuji, Effect of annealing on the mechanical properties of PLA/PCL and PLA/PCL/LTI polymer blends, *J. Mech. Behav. Biomed. Mater.* 4 (2011) 255–260.
- [50] M.P. Arrieta, J. López, E. Rayón, A. Jiménez, Disintegrability under composting conditions of plasticized PLA–PHB blends, *Polym. Degrad. Stabil.* 108 (2014) 307–318.
- [51] E. Fortunati, D. Puglia, C. Santulli, F. Sarasini, J. Kenny, Biodegradation of Phormium tenax/poly (lactic acid) composites, *J. Appl. Polym. Sci.* (2012) 125.
- [52] M. Arrieta, J. López, D. López, J. Kenny, L. Peponi, Effect of chitosan and catechin addition on the structural, thermal, mechanical and disintegration properties of plasticized electrospun PLA-PHB bionanocomposites, *Polym. Degrad. Stabil.* 132 (2016) 145–156.
- [53] M.P. Arrieta, J. López, D. López, J. Kenny, L. Peponi, Biodegradable electrospun bionanocomposite fibers based on plasticized PLA–PHB blends reinforced with cellulose nanocrystals, *Ind. Crop. Prod.* 93 (2016) 290–301.